Nonlinear optical conductivity resulting from the local energy spectrum at the *M* point in graphene

Zheng Liu,[1] Chao Zhang,[2,*] and J. C. Cao[1,†]

[1]*Key Laboratory of Terahertz Solid-State Technology, Shanghai Institute of Microsystem and Information Technology, Chinese Academy of Sciences, 865 Changning Road, Shanghai 200050, China*

[2]*School of Physics, University of Wollongong, New South Wales 2522, Australia*

(Received 1 March 2017; revised manuscript received 27 June 2017; published 27 July 2017)

Based on the tight-binding model we construct a nonlinear Hamiltonian to describe the effective electric system around the *M* point for the single layer graphene. The local energy spectrum at the *M* point is approximated by the perfect hyperbolic geometry, and the modification by the screening effect from the substrate is taken into account. With the method based on the concept of the Floquet states and quasienergies (FSQ) we investigate the third order nonlinear conductivity $\sigma_3(\omega)$, $\sigma_3(3\omega)$ for the different frequency ranges, respectively, in which only the $\pi - \pi^*$ bands are involved. A positive cusplike peak arises at $\hbar\omega = \varepsilon_{\rm gap}(\mathrm{M})/3$ for $\sigma_3(3\omega)$ which originates from the three-photon processes. Also, there is a peak at $\varepsilon_{\rm gap}(\mathrm{M})/2$ for $\sigma_3(\omega)$ resulting from two-photon-resonant processes. The analysis of the pole processes indicates that a self-energy-like term transition process plays a role in the nonlinear optical response, and the different transition processes interact with each other during the response to the external field. These interactions can be influenced by the polarization of the external field.

DOI: 10.1103/PhysRevB.96.035206

I. INTRODUCTION

Single-layer graphenes (SLG) have attracted considerable attention because of their new physical features such as the half-integer quantum hall effect [1], finite conductivity at zero charge carrier concentration [2], perfect quantum tunneling effect [3], and ultrahigh carrier mobility [4]. The band structure of SLG is described at low energies by a two-dimensional massless Dirac equation with linear dispersion. This property gives rise to a half integer quantum Hall effect [1] and dominates the low-energy physics. These properties promise building blocks for the technological applications in molecular electronic and optoelectronic devices. In graphene, the conduction and valance bands touch upon each other at isolated points in the Brillouin zone K and K′ and most of the works in studies of graphene are based on "massless Dirac theory" in the vicinity of the K(K′) point, where the local geometry of the energy spectrum (LGES) is isotropic. However, if we are concerned with the optical properties of graphene in the high frequency region more attention has to be paid to the band structure around the *M* point where the LGES is strongly twisted to be like a saddle surface [see the inset of Fig. 1(a)]. Especially, the optical conductivity induced by elementary electronic excitation is one of the central quantities to determine almost all optical properties of an electron system. It has been reported that graphene has an exceptionally high nonlinear response at visible and near infrared frequencies, which originates from the interband electron transitions [5]. The large optical nonlinearity of graphene can be used for exceptionally high-contrast imaging of single and multilayered graphene flakes. Moreover, the laser with short wavelength around the deep-ultraviolet region has been achieved experimentally [6–8], which provides the available source in practice for the application of graphene at high frequency. In this work we focus on the property of the nonlinear optical conductivity based on the interband transition around the *M* point where the energy gap $\varepsilon_{\rm gap}(M)$ is about twice the hopping energy. The Bloch states of the electron around the *M* point that live in the saddlelike surface are expected to have the special effect on the nonlinear optical response involving the resonance processes around the *M* point because of the local geometrically singularity.

In this paper the third nonlinear conductivity resulting from the local energy spectrum at the *M* point in the Brillouin zone is derived based on the tight-binding model and the Floquet theory. The results show that when the single-layer graphene is driven periodically by the weak external field the negative nonlinear conductivity (the negative real part or the negative imaginary part) arises in some frequency windows in which the multiple photons nonlinearly resonate with the electrons on the $\pi - \pi^*$ band around the *M* point. Moreover, the nonlinear conductivity curve is abrupt at the multiplephoton resonance energy. These effects might be used in graphene-based quantum nonlinear optical device where transient nonlinear gain is required such as the single photon switch based on graphene plasmons [9] or the photon blockade in the nonlinear optical microcavity [10].

II. MODEL AND METHOD

The single-layer graphene samples are usually prepared by chemical vapor deposition on the substrates such as quartz, hexagonal boron nitride (BN), and 4H-SiC, which modifies the background's dielectric constant from $\epsilon_B = 1$ to $\epsilon'_B = 1 + \Delta\epsilon(\Delta\epsilon > 0)$ [11–13]. To phenomenologically characterize the dielectric screening effect of the substrates we introduce the reduced hopping energy $t_h^R = \gamma t_h$, where $\gamma \leqslant 1(t_h = 2.7$ eV) [13]. In the tight-binding model the Hamiltonian of the single sheet of graphene can be expressed as

$$\mathrm{H}_0 = t_h^R \begin{pmatrix} 0 & \varphi_0 \\ \varphi_0^* & 0 \end{pmatrix}, \tag{1}$$

where $\varphi_0 = e^{\frac{iak_y}{\sqrt{3}}}[1 + 2e^{-\frac{1}{2}i\sqrt{3}ak_y}\cos(\frac{ak_x}{2})]$, where a is the lattice constant. The representation basis is $\langle\vec{r}|\hat{C}^\dagger_{\vec{k}_v}|0\rangle \equiv |\varphi_{\vec{k}_v}(\vec{r})\rangle = \frac{1}{\sqrt{N}}\sum_{\vec{l}_v\in T_v} e^{i\vec{k}\cdot\vec{l}_v}\phi_{2p_z}(\vec{r} - \vec{l}_v)$, $\phi_{2p_z}(\vec{r})$ is usually chosen as the $2p_z$ orbit wave function of the carbon atom. To

*czhang@uow.edu.au
†jccao@mail.sim.ac.cn

 ©2017 American Physical Society

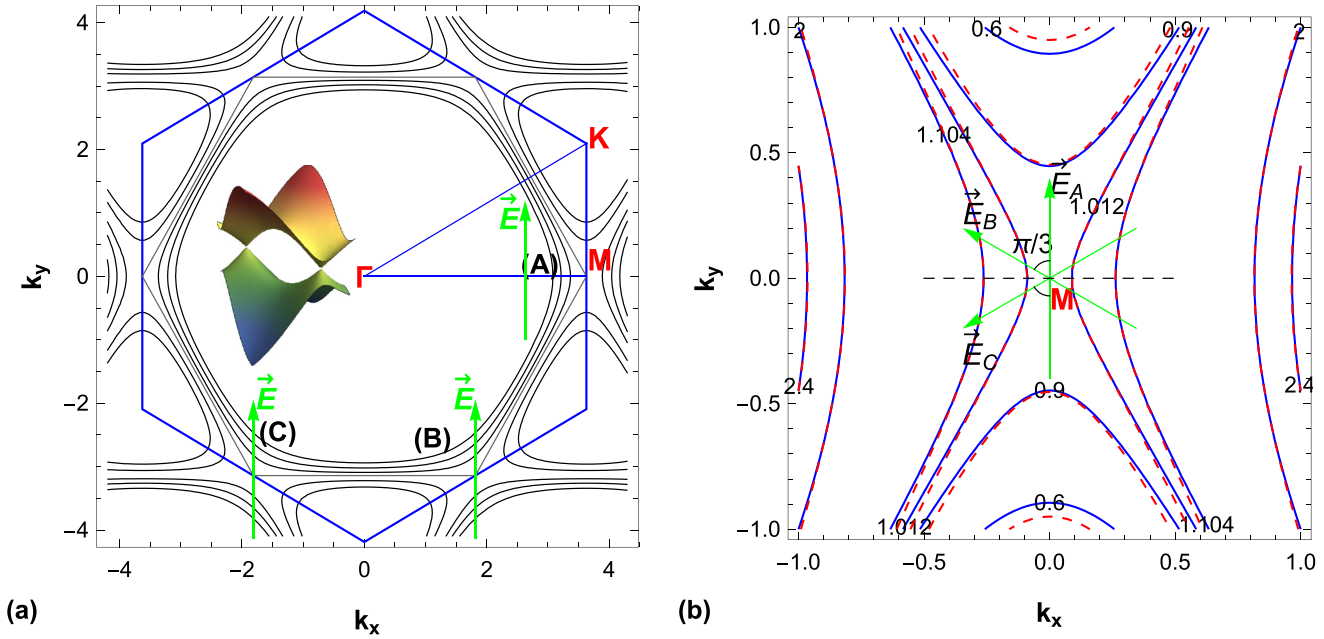

FIG. 1. The scheme of equienergy contours for the single graphene. (a) Three classes of configurations (A), (B), (C) between the external field and the local geometry of energy spectrum. (b) Constant-$\tilde{\varepsilon}^2$ contours for Eq. (3) (red dashed lines) and for Eq. (4) (blue lines).

explore the nonlinear property around the M point $\vec{k}_M = (\pi, \frac{\pi}{\sqrt{3}})\frac{1}{a}$ we expand φ_0 around the point M to the second order of $\delta k_x, \delta k_y$ and substitute the symbol $\delta\vec{k} \to \vec{p}$. In the new local coordinate system where the origin is shifted to the M point with a $\pi/6$ rotation the effective Hamiltonian in the neighborhood of the M point is written as

$$\begin{aligned} \mathrm{H}_{\mathrm{eff,M}} &= v_F \begin{pmatrix} 0 & p_- \\ p_+ & 0 \end{pmatrix} \\ &= v_F \begin{pmatrix} 0 & q_x - iq_y \\ q_x + iq_y & 0 \end{pmatrix} \end{aligned} \tag{2}$$

where $p_- = (p_+)^* = q_x - iq_y, q_x = \frac{1}{12\sqrt{3}} p_0(\tilde{p}_x^2 - 24\tilde{p}_x - 3\tilde{p}_y^2 + 12) = \tilde{q}_x p_0, q_y = \frac{1}{12} p_0(\tilde{p}_x^2 + 8\tilde{p}_x - 3\tilde{p}_y^2 + 12) = \tilde{q}_y p_0$ with the definition $p_0 = \hbar/a$, $\tilde{p}_x = p_x/p_0$, $\tilde{p}_y = p_y/p_0$ and the relation $\frac{\sqrt{3}}{2} t_h^R a = \gamma v_F \hbar \equiv v_F^R \hbar$ is used [14]. Here v_F^R is the corresponding reduced Fermi velocity and $\vec{p} = \hbar\delta\vec{k}$ is the momentum vector relative to the M point. For our two-level system periodically driven by the external fields we use the method based on the concept of the Floquet states and quasienergies (FSQ) [15–18] to calculate the relative physical quantities.

The eigenvalue and eigenvector of Eq. (2) are

$$\begin{aligned} \tilde{\varepsilon}^2 = \varepsilon^2/\left(t_h^R\right)^2 &= \frac{p_- p_+ \left(v_F^R\right)^2}{\left(t_h^R\right)^2} = \frac{3}{4}\left(\tilde{q}_x^2 + \tilde{q}_y^2\right) = \frac{3}{4}\tilde{q}^2 \\ &= 1 + \frac{3\tilde{p}_x^2}{2} - \frac{\tilde{p}_y^2}{2} + \frac{\tilde{p}_y^4}{16} + \frac{\tilde{p}_x^4}{144} - \frac{1}{24}\tilde{p}_x^2\tilde{p}_y^2 \end{aligned} \tag{3}$$

and $\begin{bmatrix} \tilde{\psi}_1 \\ \tilde{\psi}_2 \end{bmatrix} = \begin{bmatrix} \alpha_0 \\ \beta_0 \end{bmatrix} = \frac{1}{\sqrt{2}} \begin{bmatrix} e^{\pm i\phi(p)} \\ 1 \end{bmatrix}$, where $e^{i\phi(p)} = \left[\frac{p_-}{(p_-)^*}\right]^{1/2} = \left[\frac{(p_-)^2}{|p_-|^2}\right]^{1/2} = \frac{p_-}{|p_-|}$. Here it is taken that $\beta_0 = \frac{1}{\sqrt{2}}, \alpha_0 = \frac{p_-}{\sqrt{2}q}$, where $q^2 = p_+ p_- = q_x^2 + q_y^2$. The constant-$\tilde{\varepsilon}^2$ contour for Eq. (3) is shown in Fig. 1(b) with the red dashed line and in Fig. 1(a). According to the definition $\vec{v} = \nabla_{\vec{p}} \mathrm{H}_{\mathrm{couple}}$ the corresponding velocity operator is obtained and it reads $\hat{v}_{x(y)} = v_F^R \begin{pmatrix} 0 & \tilde{v}_{x(y)} \\ \tilde{v}_{x(y)}^* & 0 \end{pmatrix}$, where $\tilde{v}_x = \frac{1}{18}(\sqrt{3} + 3i)\tilde{p}_x - \frac{2}{3}(\sqrt{3} - i)$, $\tilde{v}_y = \frac{1}{6}(-\sqrt{3} - 3i)\tilde{p}_y$ by ignoring the non-Hermitian time-oscillating term. For the energy spectrum around the M point we make the important approximation by neglecting the fourth power of $\tilde{p}_x, \tilde{p}_y$:

$$\tilde{\varepsilon}^2 \approx \frac{3\tilde{p}_x^2}{2} - \frac{\tilde{p}_y^2}{2} + 1 \tag{4}$$

and limit that $|\tilde{p}_x| < 1, |\tilde{p}_y| < 1$. It is a hyperbola equation for the fixed $\tilde{\varepsilon}$ with its semimajor axis on the $\tilde{p}_x$ axis ($\tilde{\varepsilon}^2 > 1$) or on the $\tilde{p}_y$ axis ($\tilde{\varepsilon}^2 < 1$). The constant-$\tilde{\varepsilon}^2$ for Eq. (4) is shown in Fig. 1(b) with blue lines.

When the external field of the form $\vec{E} = \vec{E}_0 e^{i\omega t} = (E_{0x}\vec{e}_x + E_{0y}\vec{e}_y)e^{i\omega t}$ is applied to the system characterized by the Hamiltonian Eq. (2) the coupled Hamiltonian can be obtained by the substitution $\hat{\vec{p}} \to \hat{\vec{p}} - e\vec{A}(r,t)\hat{I}$ with $\vec{E} = -\frac{\partial \vec{A}}{\partial t}$ according to the principle of minimal electromagnetic coupling, where $\hat{p}$ is canonical momentum, $\hat{I}$ is the unit operator, and e is a scalar charge. After the substitution $p_x \to p_x - eA_x$, $p_y \to p_y - eA_y$ we get the coupled Hamiltonian

$$\mathrm{H}_{\mathrm{couple}} = v_F^R \begin{pmatrix} 0 & p_- + \xi_1 i e^{i\omega t} + \xi_2 e^{i2\omega t} \\ p_+ + \xi_1^* i e^{i\omega t} + \xi_2^* e^{i2\omega t} & 0 \end{pmatrix}, \tag{5}$$

where the momentums $\xi_1 = \xi_{1x} + \xi_{1y}, \xi_{1x} = [\frac{1}{36}(\sqrt{3}+3i)\tilde{p}_x + \frac{1}{3}(-\sqrt{3}+i)]\tilde{\xi}_{0x}p_0$, $\xi_{1y} = -(\frac{\sqrt{3}}{12} + \frac{i}{4})\tilde{p}_y\tilde{\xi}_{0y}p_0, \xi_2 = \xi_{2x} + \xi_{2y}$, $\xi_{2x} = -(\frac{1}{48\sqrt{3}} + i\frac{1}{48})\tilde{\xi}_{0x}^2 p_0, \xi_{2y} = (\frac{1}{16\sqrt{3}} + i\frac{1}{16})\tilde{\xi}_{0y}^2 p_0$ with the dimensionless parameters $\tilde{\xi}_{0x} = \frac{2eE_{0x}}{p_0\omega}$ and $\tilde{\xi}_{0y} = \frac{2eE_{0y}}{p_0\omega}$. Due to the time oscillating terms $e^{i\omega t}, e^{i2\omega t}$ the two components of the wave function $\psi(p,t)$ satisfies the Hill's Equation [19], respectively, and the related wave function $\psi(p,t)$ can be expressed as the product of an oscillating term $e^{-\frac{i}{\hbar}\varepsilon t}$ and the periodic function $\tilde{\psi}(t+T) = \tilde{\psi}(t)$ with the period $T = \frac{2\pi}{\omega}$ according to the Floquet's theorem [15–17]

$$\psi(p,t) = \begin{pmatrix}\tilde{\psi}_1(p,t)\\ \tilde{\psi}_2(p,t)\end{pmatrix} e^{-\frac{i}{\hbar}\varepsilon t} = \sum_{n=0}^{\infty}\begin{pmatrix}\alpha_n(p)\\ \beta_n(p)\end{pmatrix} e^{\frac{i(n\hbar\omega-\varepsilon)t}{\hbar}}, \tag{6}$$

where ε is independent of the electric field according to the Hellmann-Feynman theorem [17]. For the velocity operator denoted with $\hat{v} = v_F^R\begin{pmatrix}0 & \tilde{v}\\ \tilde{v}^* & 0\end{pmatrix}$, where $\tilde{v}$ is dimensionless and complex, the mean value is $\langle\hat{v}\rangle(p,t) = \psi^\dagger(p,t)\hat{v}\psi(p,t) = v_F^R(\tilde{v}\tilde{\psi}_1^*\tilde{\psi}_2 + \tilde{v}^*\tilde{\psi}_1\tilde{\psi}_2^*)$. The mean value of the total electric current is

$$\begin{aligned} J &= \frac{e}{2\pi^2\hbar^2}\int\langle\hat{v}\rangle(\vec{p},t)N_F(p)d\vec{p}\\ &= \frac{ev_F^R}{\pi^2\hbar^2}\sum_{N=1}^{\infty}\sum_{\substack{n,m=0\\ m>n\\ m+n=N}}^{\infty}\int \mathrm{Re}\big[(\alpha_n^*\beta_m\tilde{v} + \alpha_m\beta_n^*\tilde{v}^*)\\ &\quad\times e^{i(m-n)\omega t}\big]N_F(p)d\vec{p}\\ &= \sum_N J^{(N)}(t) \end{aligned} \tag{7}$$

where the Nth order current $j^{(N)} \propto E_{j_1}E_{j_2}...E_{j_N}$ with the index $j_1, j_2, ...j_N = x, y$ and $n+m=N$ is a positive odd number (time-reversal symmetry). $N_F(\tilde{\varepsilon}) = n_F(-\tilde{\varepsilon}) - n_F(\tilde{\varepsilon})$ is the thermal factor.

To check the validity of the method we calculate the linear conductivity. In the single layer graphene, the hexagonal lattice has D_{6h} symmetry which results in $\sigma_{xx}^{(1)} = \sigma_{yy}^{(1)} \equiv \sigma_1(\omega)$ and $\sigma_{xxxx}^{(3)} = \sigma_{yyyy}^{(3)}$ [20], where the nonlinear conductivity is defined by $J_y^{(3)} \propto \sigma_{yyyy}^{(3)}E_y^3$. Here we pay attention to the property of $\sigma_{yyyy}^{(3)} \equiv \sigma_3(\omega) + \sigma_3(3\omega)$. According to Eq. (7), Eq. (A4), and Eq. (A1) (see the Appendix) the corresponding linear current is obtained as

$$\begin{aligned} J_y^{(1)}(\tilde{\omega},t) &= J_0\mathrm{Re}\left[\int(\tilde{v}\alpha_0^*\beta_1 + \tilde{v}^*\alpha_1\beta_0^*)N_F(\tilde{\varepsilon})e^{i\tilde{\omega}t}d\tilde{p}_x d\tilde{p}_y\right]\\ &= J_0\mathrm{Re}\left[\frac{i}{16\tilde{\omega}}\int\frac{4\tilde{\varepsilon}(\tilde{\omega}-\tilde{\varepsilon})(\tilde{\xi}\tilde{v}^* + \tilde{\xi}^*\tilde{v}) - 3\left(\tilde{p}_-^2\tilde{\xi}^*\tilde{v}^* + \tilde{\xi}\,\tilde{p}_+^2\tilde{v}\right)}{(\tilde{\varepsilon}-\tilde{\omega}/2)}e^{i\tilde{\omega}t}d\tilde{\varepsilon}_x d\chi\right], \end{aligned} \tag{8}$$

where $\tilde{\omega} = \hbar\omega/t_h^R$, $\tilde{p}_- = p_-/p_0$, $\tilde{p}_+ = p_+/p_0$, and $J_0 = \frac{ev_F^R p_0^2}{\pi^2\hbar^2}$. With the Sokhotski-Plemelj formula the real part of the conductivity can be extracted directly form Eq. (8) and the imaginary part is obtained by numerically computing the principal value integral. The results are shown in Fig. 2, where the thermal factor is taken as $N_F(\tilde{\varepsilon}) \simeq 1$ for the low temperature approximation. It is consistent with the one with the chemical potential $\mu = 0$ in Ref. [21] where the linear conductivity is calculated with the Kubo formula. It can be found that there is clearly a typical cusplike peak at the resonance energy $2t_h^R$, which results from the abnormally high joint density of state for electron-hole excitations around M point because of the van Hove singularity. For the third order conductivity $\sigma_{yyyy}^{(3)}(\omega)$ with single frequency the corresponding current is written as

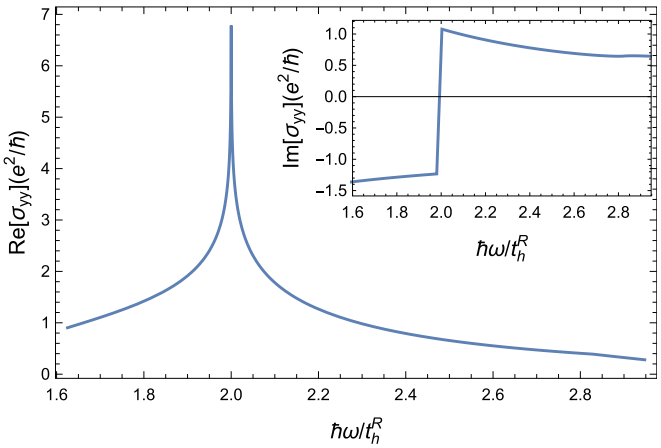

FIG. 2. The linear optical conductivity $\sigma_{yy}(\omega)$ vs frequency calculated with the FSQ method.

$$\begin{aligned} J_y^{(3)}(\tilde{\omega},t) &= J_0\mathrm{Re}\left[\int(\tilde{v}\alpha_1^*\beta_2 + \tilde{v}^*\alpha_2\beta_1^*)e^{i\tilde{\omega}t}N_F(\tilde{\varepsilon})d\tilde{p}_x d\tilde{p}_y\right]\\ &= J_0\mathrm{Re}\left[\int\frac{(-i)f(\tilde{\varepsilon},\chi,\tilde{\omega})e^{i\tilde{\omega}t}}{(\tilde{\varepsilon}-\tilde{\omega})(\tilde{\varepsilon}-\tilde{\omega}/2)^2}N_F(\tilde{\varepsilon})d\tilde{\varepsilon}d\chi\right], \end{aligned} \tag{9}$$

where the $f(\tilde{\varepsilon},\chi,\tilde{\omega})$ is a complicated real-analytic polynomial about $\tilde{p}_x, \tilde{p}_y$ and obtained by ignoring the terms the power of which are higher than four(note that $\tilde{p}_\pm$ is complex). It was noticeable that the singulary point $\tilde{\varepsilon} = \frac{\tilde{\omega}}{2}$ arises in the denominator as the second-order pole, which can cause the divergence of the integral. Therefore, the second-order pole $\frac{\tilde{\omega}}{2}$ should be outside the integral interval $\tilde{\varepsilon} \in [\frac{\sqrt{2}}{2}, \sqrt{\frac{5}{2}}]$ which is expressed as $\tilde{\omega} < \sqrt{2}$ or $\tilde{\omega} > \sqrt{10}$. On the other hand, to get the nonzero integration it is demanded that $\frac{\sqrt{2}}{2} < \tilde{\omega} < \sqrt{\frac{5}{2}}$ for

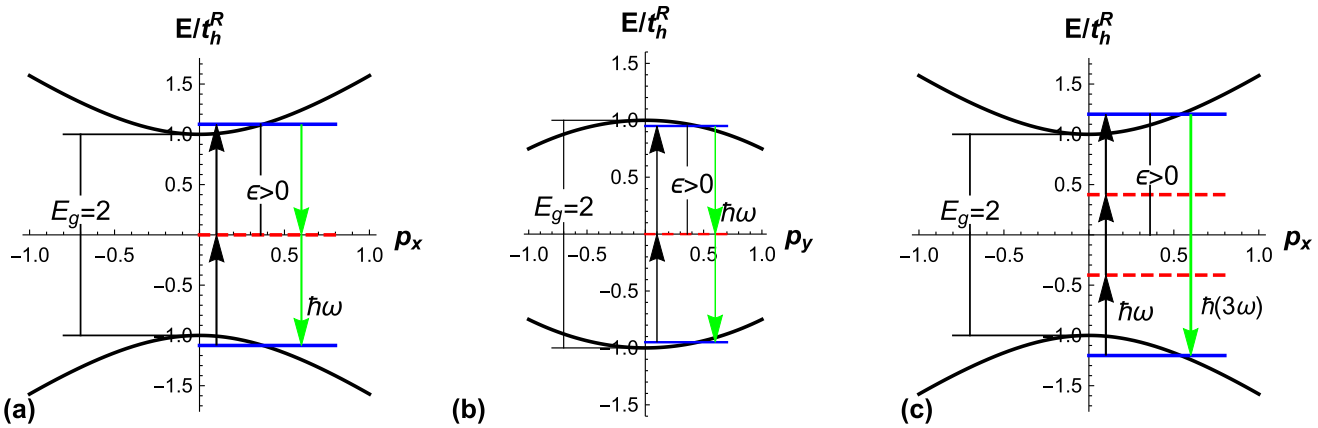

FIG. 3. The resonance structure for $\sigma_3(\omega)$ and $\sigma_3(3\omega)$. The two-photon-resonant process for the case $\sigma_3(\omega)$ in the vertical section across $\Gamma-M$ (a) and the vertical section across K-M (b). (c) The third-harmonic generation for $\sigma_3(3\omega)$ in the vertical section across $\Gamma-M$. Red dashed line: virtual level.

the single pole $\tilde{\varepsilon} = \tilde{\omega}$. So the valid range of the frequency only for the $\sigma_3(\tilde{\omega})$ case in our geometric model is $1/\sqrt{2} < \tilde{\omega} < \sqrt{2}$. For the case of $\sigma_3(\tilde{\omega})$ it is identified by the two photon processes where two incoming photons are absorbed, followed by the immediate emission of a third photon. The possible resonance structures of this type of two-photon process are shown in Fig. 3 where some virtual transitions are involved. Figures 3(a) and 3(b) correspond to a two-photon-resonance process for the two kinds of frequency range, where the energy of the photons fall into the interval $2\hbar\omega \sim \varepsilon_{\rm gap} \pm \delta\varepsilon(\delta\varepsilon > 0)$, respectively. It implies that the dominant contributions to $\sigma_3(\omega)$ come from the Bloch states above [Fig. 3(a)] or below [Fig. 3(b)] the saddle point. For the upper limit of the valid range $\tilde{\omega} = \sqrt{2}, \hbar\omega = \sqrt{2}t_h^R = 3.25$ eV, $\lambda \simeq 380$ nm, and in the range there are many types of lasers with short wavelength which can be achieved technically [6–8].

Accomplishing the calculation of Eq. (9), the third nonlinear conductivity with single frequency $\sigma_3(\tilde{\omega})$ is obtained and shown in Fig. 4. There is obviously a peak at $\tilde{\omega} = 1$, which results from the simple pole process $\tilde{\varepsilon} = \tilde{\omega}$ with the real photon emitted (two-photon resonance). It is noted that there is a small frequency window $0.7 \sim 0.75$, where $\mathrm{Re}[\sigma_3(\tilde{\omega})] < 0$. With the increase of the frequency in the resonant range the phase continually accumulates. This result is quite different from the traditional formula [5,20] in the low frequency range which is proportional to $\tilde{\omega}^{-4}$. In that case the main contributions come from the electrons around the Dirac points. However, in the high frequency range we explore the main contribution originates from the interband resonance around the M point where the local saddle-surface-like geometry manifests the hyperbolic singularity.

For the third harmonic generation $\sigma_3(3\omega)$ the corresponding third current is expressed as

$$J_y^{(3)}(3\tilde{\omega},t) = J_0\mathrm{Re}\left[\int \left(\tilde{v}\alpha_0^*\beta_3 + \tilde{v}^*\alpha_3\beta_0^*\right)e^{i3\tilde{\omega}t}N_F(\tilde{\varepsilon})d\tilde{p}_x d\tilde{p}_y\right]$$
$$= J_0\mathrm{Re}\left[\int \frac{(-i)g(\tilde{p}_x,\tilde{p}_y)e^{i3\tilde{\omega}t}}{(\tilde{\varepsilon}-\tilde{\omega})(2\tilde{\varepsilon}-\tilde{\omega})(2\tilde{\varepsilon}-3\tilde{\omega})} \times N_F(\tilde{\varepsilon})d\tilde{\varepsilon}_x d\chi\right], \quad (10)$$

where $g(\tilde{p}_x,\tilde{p}_y)$ is also a complicated real-analytic polynomial about $\tilde{p}_x,\tilde{p}_y$ and obtained by neglecting the terms the power of which are higher than four. Note that there are three simple poles in Eq. (10) $\tilde{\varepsilon} = \frac{3\tilde{\omega}}{2}, \tilde{\omega}, \frac{\tilde{\omega}}{2}$. For the pole $\tilde{\varepsilon} = \frac{3\tilde{\omega}}{2}$ it corresponds to simultaneous absorption of three photons, and this process emits a real photon with the frequency 3ω. Since

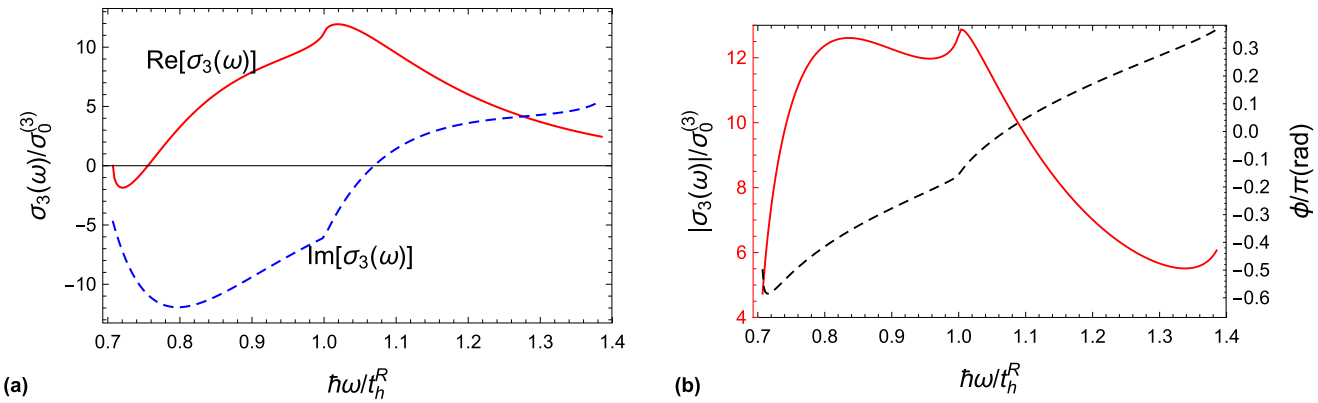

FIG. 4. Third nonlinear conductivity with single frequency $\sigma_3(\omega)/\sigma_0^{(3)} = \tilde{\sigma}_3$, where $\sigma_0^{(3)} = \frac{e^2\hbar^2(v_F^R)^2}{(t_h^R)^4}\sigma_0$ and $\sigma_0 = \frac{e^2}{4\hbar}$ (a) The real (solid line) and imaginary (dashed line) part of $\sigma_3(\omega)$ vs frequency (b) The modulus (solid line) and the phase (dashed line) $\sigma_3(\omega) = |\sigma_3(\omega)|e^{i\phi}$ vs frequency.

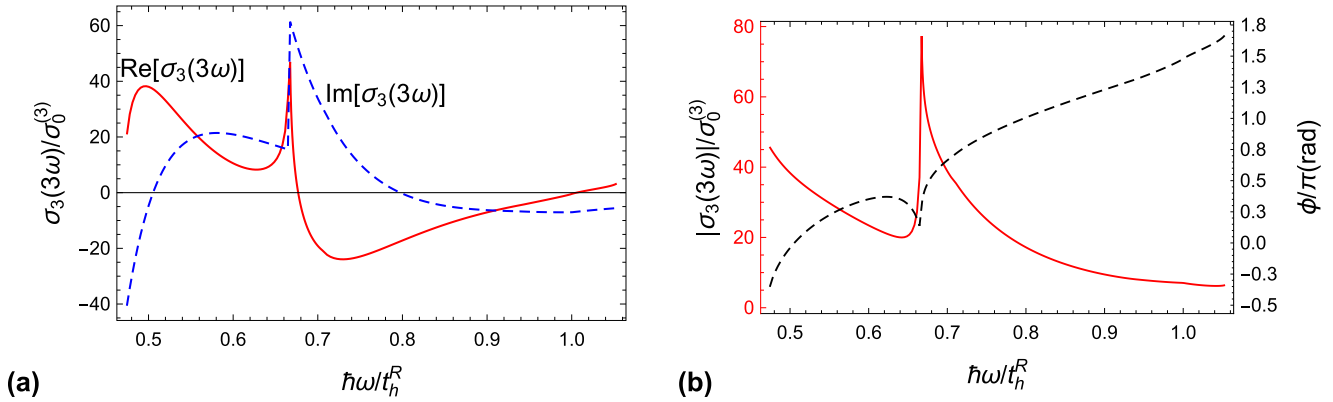

FIG. 5. Third nonlinear conductivity with single frequency $\sigma_3(3\omega)/\sigma_0^{(3)} = \tilde{\sigma}_3$. (a) The real (solid line) and imaginary part (dashed line) of $\sigma_3(3\omega)$ vs frequency. (b) The modulus (solid line) and the phase (dashed line) $\sigma_3(3\omega) = |\sigma_3(3\omega)|e^{i\phi}$ vs frequency.

there is only an oscillatory term $e^{i3\omega t}$ in the case of $\sigma_3(3\omega)$, the simple-pole processes $\tilde{\varepsilon} = \tilde{\omega}, \frac{\tilde{\omega}}{2}$ contribute to the conductivity in the way as a self-energy term process does where no real photons are emitted. The corresponding resonance structures of this type is shown in Fig. 3(c) where some virtual transitions are involved.

To get the nonzero integral value for Eq. (10) there should be at least one simple pole within the energy range $[\frac{\sqrt{2}}{2}, \sqrt{\frac{5}{2}}]$. Due to the sequence $\frac{3\tilde{\omega}}{2} > \tilde{\omega} > \frac{\tilde{\omega}}{2}$, third-harmonic generation conductivity $\sigma_3(3\tilde{\omega})$ is also a piecewise continuous function where the subdomains of $\tilde{\omega}$ are determined by how many poles and which poles fall into the interval $\tilde{\varepsilon} \in [\frac{\sqrt{2}}{2}, \sqrt{\frac{5}{2}}]$. The interval is divided into $[\frac{\sqrt{2}}{3}, \frac{2}{3}] \cup [\frac{2}{3}, \frac{\sqrt{2}}{2}] \cup [\frac{\sqrt{2}}{2}, \frac{2\sqrt{2}}{3}] \cup [\frac{2\sqrt{2}}{3}, 1] \cup [1, \sqrt{\frac{10}{9}}]$ to restrict three-photon resonance within the $\pi - \pi^*$ bands. After completing the integral of Eq. (10) in the integral domain $(\tilde{\varepsilon}, \chi) \in \Sigma$ the third-harmonic generation conductivity $\sigma_3(\tilde{\omega})$ is shown in Fig. 5. It is found that there is a cusplike positive maximum at $\tilde{\omega}_0 = 2/3$ which obviously originates from the three-photon resonance at the gap $\varepsilon_g(M) \approx 2t_h^R$. There is also a frequency range $0.68 \sim 1$ in which $\mathrm{Re}[\sigma_3(\tilde{\omega})]$ is negative and it is thought to be the effect by the self-energy-like process $\tilde{\varepsilon} = \tilde{\omega}$. The phase basically ascends continuously with the increase of the frequency except the points around $\tilde{\omega}_0 = 2/3$, where nonlinear multiphoton resonance occurs at the cost of the phase defect.

Because of the singularity of the saddle-surface-like geometry of the local energy spectrum at the M point, which has no rotational symmetry, when the external field with different polarization is applied to the system it is expected that the different nonlinear response will be excited. In Fig. 6 it gives the third-harmonic generation conductivities contributed by the local geometric spectrum only from the configuration, which is defined as the relative orientation between the local energy spectrum geometry and the external field polarization, (A) $\sigma_3^{\mathrm{A}}(\tilde{\omega})$ or only from the configuration (B) (same to C) $\sigma_3^{\mathrm{B}}(\tilde{\omega})$ (see Fig. 1) and the distribution of the group velocity without external field is sketched in the inset. It is noted that contribution from the the configuration (A) is much larger than the one from configuration (B) and the resonance peak arises for the configuration (B). It is implied that nonlinear multiphoton resonance is dependent on the polarization of the external field. As is shown in the inset, the distribution of the group velocity is centrosymmetric when there is no external field and the net charge current is therefore zero. The polarization in the configuration (B) destroys the symmetry of the local electric system much more severely than the one in the configuration (A).

III. CONCLUSIONS

In summary, we construct a nonlinear Hamiltonian based on the tight-bind method to characterize the local electric system around the M point in the Brillouin zone of the single layer graphene. By approximating the local energy band structure as the perfect hyperbolic geometry and using the FSQ method we investigate the third-harmonic generation $\sigma_3(3\omega)$ and single-frequency nonlinear conductivity $\sigma_3(\omega)$ in different frequency ranges, respectively, where the nonlinear multiphoton resonances take place only between the $\pi - \pi^*$ bands. In the calculation the screening effect from the substrate is taken into account by introducing the reduced parameters. As one anticipated there exist a positive cusplike peak at $\hbar\omega = E_{\mathrm{gap}}(M)/3$ for $\sigma_3(\omega)$ and a peak at $E_{\mathrm{gap}}(M)/2$ for $\sigma_3(\omega)$ which originate from the nonlinear multiphoton resonance physically. The corresponding phase continually accumulates

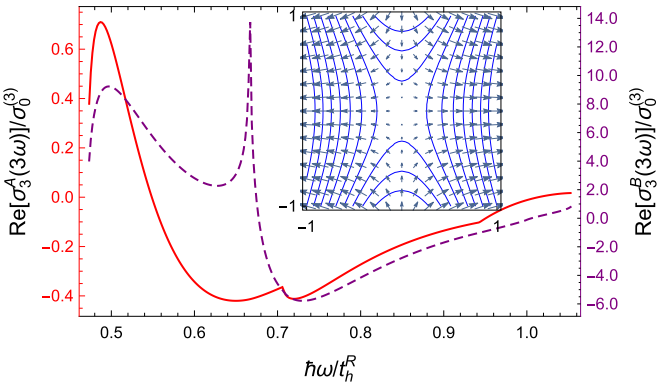

FIG. 6. The third-harmonic generation conductivity for different effective field polarization $\sigma_3^{\mathrm{A}}(\tilde{\omega}), \sigma_3^{\mathrm{B}}(\tilde{\omega})$. Inset: The distribution of the group velocity around the M point.

with the increase of the frequency in the resonant range except the neighborhood of the resonance point. It is noted that there are some frequency intervals where the real part of the conductivity is negative for the third-harmonic generation or the single-frequency nonlinear conductivity. It may be attributed to the effect by the self-energy-like transition process involving the virtual levels and implies that the different transition processes (including the self-energy-like process) can interact with each other during the response to the external field. It is very similar to the situation in quantum optics where the "different-path" transitions give the coherent interference during the multiphoton radiation. Due to the anisotropy of the local energy band structure around the M point (not like the Dirac cone), for the fixed polarization of the external field there are multiple groups of electrons around the M point in the whole Brillouin zone that is classified according to the relative orientation between the local energy spectrum geometry and the external field polarization. The electrons around the M point under the different configurations may respond to the external field in a different way and the polarization of the external field can be therefore used to tune the position of the peak in the nonlinear multiphoton resonances, and this is left for future work.

ACKNOWLEDGMENTS

This work was supported by the 973 Program of China (Grant No. 2014CB339803), the National Natural Science Foundation of China (Grant No. 61404150), and the Shanghai Municipal Commission of Science and Technology (Project No. 15JC1403800), and the Australian Research Council Grant through a Discovery Grant (DP160101474).

APPENDIX: DERIVATION OF THE N ORDER CURRENT

After substituting Eq. (6) and Eq. (5) into the Schrödinger equation we obtain the recurrence equations which is very similar to the one in Refs. [22–25]

$$\begin{aligned}\alpha_n(\varepsilon - n\omega\hbar) &= p_- v_F^R \beta_n + i\xi_1 v_F^R \beta_{n-1} + \xi_2 v_F^R \beta_{n-2}\\ \beta_n(\varepsilon - n\omega\hbar) &= p_+ v_F^R \alpha_n + i\xi_1^* v_F^R \alpha_{n-1} + \xi_2^* v_F^R \alpha_{n-2}\end{aligned} \tag{A1}$$

for $n \geqslant 1$ and $\alpha_0\varepsilon = v_F^R \beta_0 p_-$, $\beta_0\varepsilon = v_F^R \alpha_0 p_+$ for $n = 0$.

For the approximation Eq. (4) we make a transformation

$$\begin{aligned}\tilde{p}_x &= \sqrt{\frac{2(\tilde{\varepsilon}^2 - 1)}{3}}\cosh\chi\\ \tilde{p}_y &= \sqrt{2(\tilde{\varepsilon}^2 - 1)}\sinh\chi\end{aligned} \tag{A2}$$

for $\tilde{\varepsilon} > 1$ where $|\tilde{p}_x| < 1 \Rightarrow \tilde{\varepsilon} < \sqrt{\frac{5}{2}}$ and $\chi < \cosh^{-1}[\frac{\sqrt{3}}{\sqrt{2(\tilde{\varepsilon}^2-1)}}] = \chi^+_{\tilde{p}_x}$, $|\tilde{p}_y| < 1 \Rightarrow \chi < \sinh^{-1}[\frac{1}{\sqrt{2(\tilde{\varepsilon}^2-1)}}] = \chi^+_{\tilde{p}_y}$. Note that $\tilde{\varepsilon} > \sqrt{2}$, $\chi^+_{\tilde{p}_x} < \chi^+_{\tilde{p}_y}$ and define $\chi^+_{\max} = \mathrm{Min}(\chi^+_{\tilde{p}_x}, \chi^+_{\tilde{p}_y})$.

For $\tilde{\varepsilon} < 1$ the transformation is

$$\begin{aligned}\tilde{p}_x &= \sqrt{\frac{2(1 - \tilde{\varepsilon}^2)}{3}}\sinh\chi\\ \tilde{p}_y &= \sqrt{2(1 - \tilde{\varepsilon}^2)}\cosh\chi,\end{aligned} \tag{A3}$$

where $|\tilde{p}_y| < 1 \Rightarrow \tilde{\varepsilon} > \frac{\sqrt{2}}{2}$ and $\chi < \cosh^{-1}[\frac{1}{\sqrt{2(1-\tilde{\varepsilon}^2)}}] = \chi^-_{\tilde{p}_y}$, $|\tilde{p}_x| < 1 \Rightarrow \chi < \sinh^{-1}[\frac{\sqrt{3}}{\sqrt{2(1-\tilde{\varepsilon}^2)}}] = \chi^-_{\tilde{p}_x}$. Note that $\tilde{\varepsilon} > 0$, $\chi^-_{\tilde{p}_y} < \chi^-_{\tilde{p}_x}$ and define $\chi^-_{\max} = \mathrm{Min}(\chi^-_{\tilde{p}_x}, \chi^-_{\tilde{p}_y})$.

The real part of the Nth order nonlinear conductivity can be extracted by calculating

$$\begin{aligned}J^{(N)}_{j_0}(t)|_{t=0} &= \mathrm{Re}\big[\sigma^{(N)}_{j_0,j_1,\ldots j_N}(\omega_1,\omega_2,\ldots\omega_N)E_{j_1}E_{j_2}\ldots E_{j_N}\big]\\ &= \mathrm{Re}\left[\iint_\Sigma f(\tilde{p}_x,\tilde{p}_y)\frac{2\tilde{\varepsilon}}{\sqrt{3}}d\tilde{\varepsilon}d\chi\right]J_0\\ &= \mathrm{Re}\left[\lim_{\delta\to 0}\int_{1/\sqrt{2}}^{\sqrt{5/2}}\frac{(-i)F(\tilde{\varepsilon},\tilde{\omega})}{\prod_n[\tilde{\varepsilon} - (\tilde{\varepsilon}_n + i\delta)]}d\tilde{\varepsilon}\right]J_0,\end{aligned} \tag{A4}$$

where $f(\tilde{p}_x,\tilde{p}_y) = N_F(\tilde{\varepsilon})\sum_{n=0}^{(N-1)/2}(v\alpha_n^*\beta_{N-n} + v^*\alpha_{N-n}\beta_n^*)$, $\Sigma := \{(\tilde{\varepsilon},\chi)\} = \Sigma_1 + \Sigma_2 + \Sigma_3$, $\Sigma_1 = [\frac{\sqrt{2}}{2},1]\times[0,\chi^-_{\tilde{p}_y}]$, $\Sigma_2 = [1,\sqrt{2}]\times[0,\chi^+_{\tilde{p}_y}]$, $\Sigma_3 = [\sqrt{2},\sqrt{\frac{5}{2}}]\times[0,\chi^+_{\tilde{p}_x}]$. The field amplitude E_{j_N} is assumed to be real and $\omega_N = \pm\omega$ for simplification. $F(\tilde{\varepsilon},\tilde{\omega})$ is a real-analytic polynomial and $\tilde{\varepsilon}_n$ is the pole like $\tilde{\omega}/2,\tilde{\omega},3\tilde{\omega}/2$. With the Sokhotski-Plemelj formula $\frac{1}{\tilde{\varepsilon}-\tilde{\omega}-i\Delta} = \mathcal{P}\frac{1}{\tilde{\varepsilon}-\tilde{\omega}} + i\pi\delta(\tilde{\varepsilon} - \tilde{\omega})$ we can get the real part directly without calculating the integral, and the imaginary part is obtained by numerically calculating the principal value integral in the range $\tilde{\varepsilon} \in [1/\sqrt{2},\sqrt{5/2}]$. For the calculation of the anisotropic conductivity it is usually assumed that there is only one electric field component for simplification. In the case of Dirac cone at $K(K')$, due to the rotational symmetry of its shape the total current is $J_{\mathrm{total}} = 6J_{\mathrm{cone}}$. When the electric field with polarization $\vec{E} = E_0\vec{e}_y$ is applied to the graphene layer there are three relative configurations between $\vec{E}$ and the hyperbolic-shaped LGES around the M point which are shown in Fig. 1(a) marked with (A), (B), (C). Because of the mirror symmetry (xy plane) case (B) and case (C) contribute the same current along the y direction $J_{\mathrm{B}} = J_{\mathrm{C}} \equiv J_{\mathrm{n}}$. In the same coordinate system with the origin at M [see Fig. 1(b)] for the external field $\vec{E} = E_0\vec{e}_y$ the effective local fields is $\vec{E}_{\mathrm{B(C)}} = |\vec{E}|\vec{n} = (-\cos\frac{\pi}{6}E_0\vec{e}_x \pm \sin\frac{\pi}{6}E_0\vec{e}_y)\vec{n}$, where $\vec{n} = -\cos\frac{\pi}{6}\vec{e}_x \pm \sin\frac{\pi}{6}\vec{e}_y$. For the case (A), $\tilde{\xi}^{\mathrm{A}}_{0x} = 0, \tilde{\xi}^{\mathrm{A}}_{0y} = \frac{2eE_0}{p_0\omega} \equiv \tilde{\xi}_0$ and for the case (B), (C) $\tilde{\xi}^{\mathrm{B(C)}}_{0x} = -\frac{\sqrt{3}}{2}\tilde{\xi}_0$, $\tilde{\xi}^{\mathrm{B(C)}}_{0y} = \pm\frac{1}{2}\tilde{\xi}_0$. The corresponding velocity operators $\hat{v}_n = \nabla_{\vec{p}}\mathrm{H}_{\mathrm{couple}}\cdot\vec{n} = \begin{pmatrix}0 & \tilde{v}_n\\ \tilde{v}_n^* & 0\end{pmatrix}$, $\tilde{v}_n = (-\frac{\sqrt{3}}{2}\tilde{v}_x \pm \frac{1}{2}\tilde{v}_y)$. The total current component along the y direction for the system is $J_{\mathrm{total}} = 2J_{\mathrm{A}} + 4J_{\mathrm{n}}$ when the y-polarized external field with the frequency around the energy $\varepsilon_{\mathrm{gap}}(M)$ is applied to the system.

[1] Y. Zhang, Y.-W. Tan, H. L. Stormer, and P. Kim, Nature (London) **438**, 201 (2005).
[2] K. S. Novoselov, A. K. Geim, S. V. Morozov, D. Jiang, M. I. Katsnelson, I. V. Grigorieva, S. V. Dubonos, and A. A. Firsov, Nature (London) **438**, 197 (2005).
[3] M. I. Katsnelson, K. S. Novoselov, and A. K. Geim, Nat. Phys. **2**, 620 (2006).
[4] A. K. Geim and K. S. Novoselov, Nat. Mater. **6**, 183 (2007).
[5] E. Hendry, P. J. Hale, J. Moger, A. K. Savchenko, and S. A. Mikhailov, Phys. Rev. Lett. **105**, 097401 (2010).
[6] Y. Taniyasu, M. Makoto Kasu, and T. Makimoto, Nature (London) **441**, 325 (2006).
[7] R. G. Banal, Y. Taniyasu, and H. Yamamoto, Appl. Phys. Lett. **105**, 053104 (2014).
[8] M. Shatalov, M. Gaevski, V. Adivarahan, and A. Khan, Jpn. J. Appl. Phys. **45**, L1286 (2006).
[9] M. Gullans, D. E. Chang, F. H. L. Koppens, F. J. García de Abajo, and M. D. Lukin, Phys. Rev. Lett. **111**, 247401 (2013).
[10] K. M. Birnbaum, A. Boca, R. Miller, A. D. Boozer, T. E. Northup, and H. J. Kimble, Nature (London) **436**, 87 (2005).
[11] C. Jang, S. Adam, J.-H. Chen, E. D. Williams, S. Das Sarma, and M. S. Fuhrer, Phys. Rev. Lett. **101**, 146805 (2008).
[12] A. Raoux, M. Polini, R. Asgari, A. R. Hamilton, R. Fazio, and A. H. MacDonald, Phys. Rev. B **81**, 073407 (2010).
[13] C. Hwang, D. A. Siegel, S.-K. Mo, W. Regan, A. Ismach, Y. Zhang, A. Zettl, and A. Lanzara, Sci. Rep. **2**, 590 (2012).
[14] P. R. Wallace, Phys. Rev. **71**, 622 (1947).
[15] J. H. Shirley, Phys. Rev. **138**, B979 (1965).
[16] R. H. Young, W. J. Deal, Jr., and N. R. Kestner, Mol. Phys. **17**, 369 (1969).
[17] H. Sambe, Phys. Rev. A **7**, 2203 (1973).
[18] F. Grossmann, T. Dittrich, P. Jung, and P. Hänggi, Phys. Rev. Lett. **67**, 516 (1991).
[19] W. Magnus and S. Winkler, *Hill's Equation* (John Wiley & Sons, New York, 1966).
[20] J. L. Cheng, N. Vermeulen, and J. E. Sipe, New J. Phys. **16**, 053014 (2014).
[21] C. Zhang, L. Chen, and Z. Ma, Phys. Rev. B **77**, 241402(R) (2008).
[22] A. R. Wright, X. G. Xu, J. C. Cao, and C. Zhang, Appl. Phys. Lett. **95**, 072101 (2009).
[23] X. G. Xu, S. Sultan, C. Zhang, and J. C. Cao, Appl. Phys. Lett. **97**, 011907 (2010).
[24] Z. Liu, M. Sanderson, J. C. Cao, and C. Zhang, Phys. Rev. B **90**, 235430 (2014).
[25] Z. Liu, M. Sanderson, C. Zhang, and J. C. Cao, J. Appl. Phys. **118**, 043106 (2015).